

## Some applications of barium titanate prepared by different methods

Volodymyr Sydorчук<sup>1</sup>, Svitlana Khalameida<sup>1</sup>, Ewa Skwarek<sup>2</sup>, Adrianna Biedrzycka<sup>2</sup>

<sup>1</sup> National Academy of Sciences in Ukraine

<sup>2</sup> Maria Curie-Skłodowska University in Lublin

Corresponding author: [ewunias@hektor.umcs.lublin.pl](mailto:ewunias@hektor.umcs.lublin.pl) (Ewa Skwarek)

**Abstract:** The paper presents some application of barium titanate synthesized by different methods. Barium titanate samples were prepared by four procedures: solid state, mechanochemical as direct synthesis and modification as well as hydrothermal and microwave. The obtained samples were systematically studied using X-ray diffraction, nitrogen adsorption, Fourier transform infrared spectroscopy (FTIR), potentiometric titration, and quasi-elastic light scattering and zeta potential measurements. The values of pHPzc (point of zero charge) and pH<sub>IEP</sub> (isoelectric point) characteristic of the electrical double layer were determined. The prepared samples were tested as photocatalysts under visible light. As a result, relationship between the conditions of barium titanate synthesis, its physicochemical and electrokinetic parameters, as well as photocatalytic activity under visible light was first established.

**Keywords:** barium titanate, synthesis, physicochemical and photocatalytic properties

### 1. Introduction

One of the most important tasks of modern fundamental and applied science is the development of processes to protect the environment from harmful gas emissions and wastewater treatment. Photocatalysis and adsorption are promising areas for creating the effective environmental technologies (Thompson and Yates, 2006; Bagheri et al., 2020). Different oxides of transition metals are used as active materials most often in such processes. Perovskites which are semiconductors can be potential photocatalysts. Barium titanate BaTiO<sub>3</sub> (BT) obtained *via* conventional solid state method or dry milling is firstly used as ferroelectric material (Rae et al., 2007; Zazhigalov et al., 2008; Gorelov et al., 2011). However, strontium and barium titanate prepared as aerogels titanate is active in gas-phase and liquid-phase processes of photooxidation of some organic pollutants (Demydov and Labaunde, 2004). There are other methods for synthesis of BT as photocatalysts, namely: sol-gel (Karthik et al., 2019), polymeric complex (Kappadan et al., 2016), hydrothermal (Bantawal et al., 2018).

It has been much less studied as a photocatalyst and moreover does not belong to typical adsorbents. At the same time, as a traditional industrial electroceramic material, it is a large-tonnage waste in the case of capacitor disposal which can be reused for other purposes (Kikuta et al., 2006). In addition to the production of titanium dioxide from spent barium titanate proposed in latter work, it is also possible to use it as a catalyst in the processes of photodegradation of pollutants. Sorption of cations from aqueous media is another possible aspect for application of spent BaTiO<sub>3</sub> which is based on results of works in which different procedures of BT synthesis were used: solid state (Guin et al., 2006; Mishra et al., 1996; Saravaia et al., 2016; Al-Hobaib and Al-Suhybani, 2014), co-precipitation (Chen et al., 2011), dealloying – ion exchange of Ti-containing alloy (Saito et al., 2019), sol-gel with ion exchange (Guevar et al., 2017), Al-Hobaib and Al-Suhybani, 2014).

Both indicated its applications (photocatalysis and sorption of cations) require knowledge of phenomena at the solid/ solution interface (particularly, the dependence of zeta potential surface charge density from pH of solution). Adsorption of substrate at the photocatalyst surface, which is the first stage of any catalytic process, depends on these parameters. These properties are highly dependent on the synthesis method of BT. For example, the authors of works (Lewis, 2000; Vamvakaki

et al., 2001; Shen et al., 2004; Blanco-Lopez et al., 2000; Hsu et al., 2005; Tripathy and Raichur, 2011; Kosmulski, 2004) were studied zeta-potential of different dispersion based on BT.

It should be noted that the photocatalytic properties of barium titanate have been studied in detail only under the action of UV irradiation (Demydov and Labaunde, 2004; Khalameida et al., 2010; Lee et al., 2013; Kaya et al., 2019; Jiao et al., 2016; Karthik et al., 2019; Pirgholi-Givi et al., 2021; Xiong et al., 2005; Kappadan et al., 2016). However, it is almost inactive under visible irradiation since BT has band gap about 3.2-3.3 eV. As a result, visible illumination does not cause excitation of electron and formation charge carriers that are necessary for the occurrence reactive oxygen species (Thompson and Yates, 2006). At the same time, stable ferroelectric tetragonal modification of BaTiO<sub>3</sub> prepared by calcinations above 1100°C has band gap about 3.1 eV and show higher absorption in visible region (Kappadan et al., 2016; Cui et al., 2013) as a result of which it becomes active under visible irradiation. In addition to these works, there are only separate studies documenting the activity of BT under these conditions (Kaya et al., 2019; Ni et al., 2015; Bantawal and Bhat, 2018; Khalameida et al., 2017). Besides, the activation of cubic barium titanate can be associated with the introduction of defects in its structure or its formation with a certain morphology of particles. For example, mechanochemical synthesis of BT which is accompanied by defect structure formation causes narrowing the band to 2.7-2.8 eV and corresponding increasing its activity in UV region (Khalameida et al., 2010). Also, photocatalytic activity of BT under visible light becomes noticeable as a result (Khalameida et al., 2017).

At the same time, studies devoted to establishing the relationship between electrokinetic characteristics of BT, on the one hand, and its photocatalytic and adsorption properties, on the other hand, are absent in the literature how is it done, for example for TiO<sub>2</sub> in works (Górska et al., 2008; Chun et al., 2001; Chen et al., 2003; Wilhelm and Stephan, 2007).

The main procedures of BT preparation are solid state reactions, including from titanyloxalate, hydrothermal, microwave and mechanochemical (Rae et al., 2007). The synthesized products differ quite strongly in their physicochemical characteristics, which are important for their use in photocatalytic and adsorption processes. These include the crystal and porous structure, specific surface area, the nature of surface functional groups, and electrokinetic characteristics (Thompson and Yates, 2006; Khalameida et al., 2010; Lee et al., 2013; Kaya et al., 2019; Jiao et al., 2016; Karthik et al., 2019; Pirgholi-Givi et al., 2021; Xiong et al., 2015; Kappadan et al., 2016; Górska et al., 2008).

In this work, we studied barium titanate samples prepared *via* indicated methods and carried out the comparative research of these parameters and their influence on the photocatalytic degradation of rhodamine B under the action of visible light. The study of electrokinetic characteristics of these barium titanate samples in the presence of Cd (II) ions in order to evaluate them as potential adsorbents is other task of this work. Such systematic investigations focused on effect of different methods barium titanate preparation on complex physicochemical and electrokinetic characteristics and, as a result, on its photocatalytic properties under visible irradiation have not been previously carried out.

## 2. Materials and methods

Analytical-grade reagents were used in presented study. These are barium titanyloxalate (Ferro), BaO (Alfa-Aesar) and amorphous TiO<sub>2</sub> (Alfa-Aesar). The samples of barium titanate were prepared by four different procedures. Solid state method is based on thermodestruction of barium titanyloxalate (BTO) at 800°C as described elsewhere (Khalameida et al., 2010; Malghe et al., 2004; Sydoruk et al., 2009). This sample was designated as SS-800. It was also modified by milling in water at 600 rpm and microwave treatment (MWT) at 250°C for 1h (samples SS-MChT-600 and SS-MWT-250, respectively). Other samples were prepared from stoichiometric mixture of BaO with X-ray amorphous TiO<sub>2</sub> (Khalameida et al., 2017). Mechanochemical sample (MChT-600 air) was synthesized by milling this mixture in air at 600 rpm for 5h (Khalameida et al., 2017; Khalameida et al., 2010; Welham, 1998). A planetary ball mill Pulverisette 6 (Fritsch GmbH) with vessel and ten balls of silicon nitride of 15 mm diameter (total mass – 130 g) was used for this purpose. Hydrothermal synthesis (HTS) was carried out in stainless steel autoclave with 45 ml volume at 250°C and under the autogeneous pressure for 5 h (HTS-250). High-pressure reactor “NANO 2000” (Plazmatronika, Poland) with the power of 650 W

was used for microwave synthesis (MWS-250 and SS-MWT-250). In this case, the treatment temperature and pressure were 250°C and 4.5 MPa, respectively. Prepared samples are listed in Table 1.

Table 1. Some characteristics of studied samples

No.	Designation	Conditions of preparation	S, m <sup>2</sup> /g	V, cm <sup>3</sup> /g	I <sub>101</sub> /I <sub>110</sub>	D <sub>101</sub> , nm	D <sub>s</sub> , nm
1	SS-800	Thermodestruction of BTO, 800°C 7h	23	0.01	3.36	16.8	43
2	MChS-600-air	MChT (TiO <sub>2</sub> +BaO) 600 rpm air 5h	14	0.05	3.18	12.0	70
3	MWS-250	MWT (TiO <sub>2</sub> +BaO) 250°C 1h	14	0.25	3.64	18.5	71
4	SS-MChT-600-H <sub>2</sub> O	MChT sample of 1 at 600 rpm H <sub>2</sub> O 1h	15	0.32	3.30	15.5	67
5	HTS-250	HTT (TiO <sub>2</sub> +BaO) 250°C 5h	6	0.21	3.60	19.6	167
6	SS-MWT-250	MWT of sample 1 at 250°C 1h	11	0.15	3.51	20.0	90

XRD measurements were performed with diffractometer PW 1830 produced by Philips using CuK $\alpha$  radiation. The crystallites size was calculated using the Sherrer formula for the most intense reflex at  $2\theta = 31.6^\circ$ :

$$D_{101}=0.9L/(B \cos \theta), \quad (1)$$

where L - wavelength of CuK $\alpha$  radiation (0.154 nm), B - reflex width at half height (radian),  $\theta$  - diffraction angle.

The FTIR spectra in the range 4000-1000 cm<sup>-1</sup> were registered by the spectrometer "Spectrum - One" produced by Perkin-Elmer (tablets with KBr at the mass ratio sample/KBr=1:20). UV-Vis spectra were registered on spectrometer Lambda 35, Perkin Elmer Instruments (standard - MgO). Absorption edge  $\lambda$  was determined from these spectra and band gap  $E_g$  was calculated using Tauc plot (Landri et al., 2022)

The specific surface area S and pore volume V were calculated from adsorption-desorption isotherms of nitrogen, which were recorded with the help of analyzer "NOVA instruments" (Quantochrome Instruments), using BET method and adsorption value at relative pressure of nitrogen close to 1. The samples were outgassed at 150°C for 2 h before measurements. EPR spectra were obtained at 20°C on spectrometer "Varian E-112" ("Varian", USA). The surface morphology was studied using High resolution Scanning Electron Microscope Quanta 3D FEG, FEI (USA).

The  $\zeta$  potential of barium titanate samples was determined by means of electrophoresis using a Zetasizer 3000 Standard (Malvern) as described elsewhere (Janusz et al., 2010). The concentration of BT in the electrolyte solution was 100 ppm. The suspension was ultrasonicated before measurements. Isoelectric point p*H*<sub>iep</sub> was determined from the dependences  $\zeta$  potential - p*H* obtained in water. The surface charge density  $\sigma$  at the BT/water interface was determined by potentiometric titration of the aqueous BT suspension. It was carried out in the thermostatic Teflon vessel, in a nitrogen atmosphere free of CO<sub>2</sub>, at 25°C. The measurements were performed using a PHM 240 Radiometer Research pH meter with K401 as a glass electrode and G202B as the calomel reference electrode. Potentiometric titration was carried out with the use of the automatic burette Dosimat (Metrohm). The point of zero charge p*H*<sub>pzc</sub> was calculated from  $\sigma$  - p*H* curves.

Besides, electrokinetic measurements were carried out in the presence of Cd (II) ions utilizing Zetasizer Nano ZS90 (Malvern) for each sample.

Photocatalytic degradation of rhodamine B (RhB) in aqueous solutions under the action of visible light was chosen as a test reaction for estimation of photocatalytic properties of prepared samples. Visible irradiation was carried out using GE Lucalox lampe (70 W, glass reactor). The emission spectrum of the used lamp is shown in Fig. 1. As can be seen, there is maximum around wavenumber 568 nm which almost coincides with maximum of absorption for RhB (553 nm). The optimum conditions for photodegradation were as follows: RhB concentration - 1·10<sup>-5</sup> mol/l, mass ratio

catalyst/solution - 1 : 1, vigorous stirring of dispersion. The value of RhB adsorption during dark stage  $a$  (%), determined as the ratio of optical density of RhB solution before and after dark stage. About a 3-ml aliquot of the dye solution was withdrawn after determined time interval and analysed spectrophotometrically at  $\lambda_{\max}=553$  nm (Lambda 35, Perkin- Elmer Instruments) after centrifugation of dispersion.

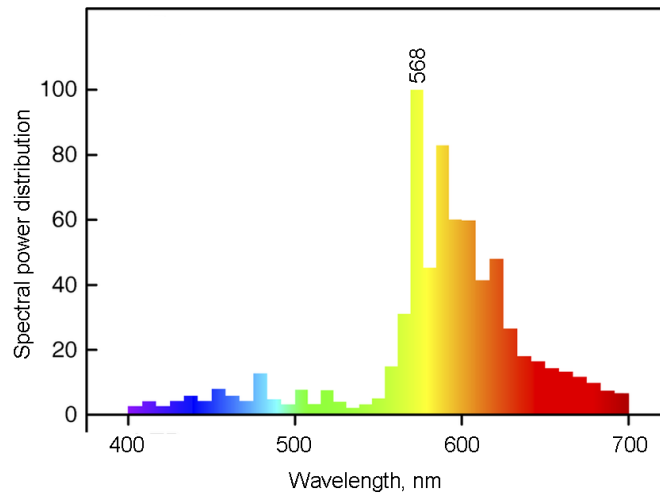


Fig. 1. The emission spectrum of used GE Lucalox lamp

### 3. Results and discussion

#### 3.1. Crystal and surface structure

As shown in Fig. 2 all prepared samples have structure of barium titanate cubic modification ((JCPDS File No. 31-0174): peaks at  $2\theta = 22.2, 31.6, 38.9, 45.3, 51.0, 56.2^\circ$ ). Besides, all samples contain minimal amount of  $\text{BaCO}_3$  as impurity ( $2\theta=24.1$  and  $34.4^\circ$ ). Based on the FWHM values for peak corresponding to plane 101, the average crystallite size of the BT samples  $D_{101}$  was calculated by a Scherrer's formula.

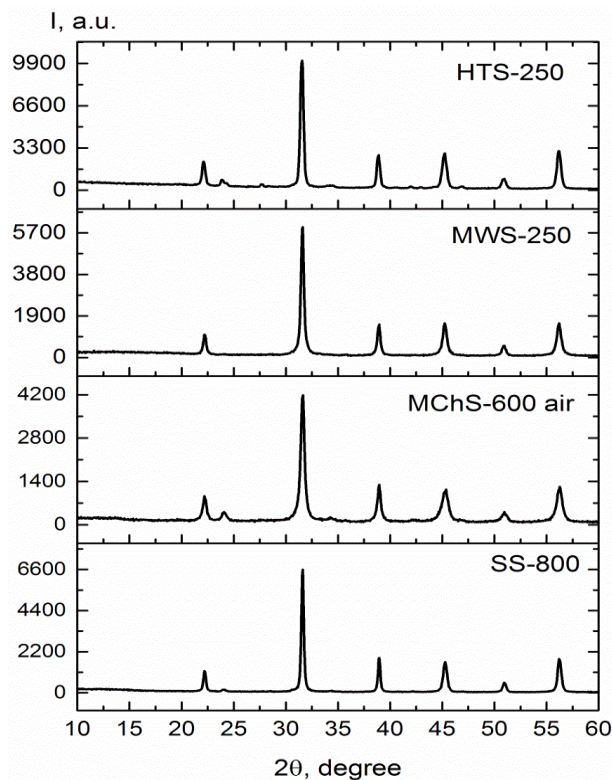


Fig. 2. XRD patterns for some samples

The magnitude of  $D_{101}$  is 12-20 nm for studied samples. At the same time, effective diameter of particles calculated using value of specific surface area  $D_s$  has significantly larger value. The ratio  $D_s/D_{101}$  can be as degree of aggregation of primary crystallites. This parameter is changed in wide limits, namely 2.6-8.5. The crystallites of samples, prepared in the presence of water, are maximally aggregated due to realization of the mechanism of dissolution-precipitation, which is possible under hydrothermal conditions. Therefore, value of specific surface area is lesser for these samples. They also have a significantly larger pore volume  $V$  than those obtained in air (Table 1). This additional porosity is represented mainly by meso- and macropores: their fraction is about 0.2-0.3 cm<sup>3</sup>/g.

Studied sample also differ in ratio of intensities of planes 101 and 110  $I_{101}/I_{110}$  which is within 3.18-3.64. The latter can affect the adsorption and photocatalytic properties of the samples (Thompson and Yates, 2006; Kaya et al., 2019). Therefore, presented results indicate some defective crystal structure of the mechanochemical sample. As can be seen from Table 1, specific surface area of studied samples is within 6-23 m<sup>2</sup>/g as in other works devoted barium titanate (Lee et al., 2013; Kaya et al., 2019; Jiao et al., 2016; Karthik et al., 2019; Xiong et al., 2015).

These defects arise on the stage of dry milling, which is already a common view (Wang et al., 2004; Indris et al., 2005; Phan et al., 2013). Particularly, this may be pair  $Ti^{3+}$  -  $V_o$  for titanium oxide compositions. Indeed, EPR spectroscopy indicates that mechanochemical BT, in contrast to samples prepared by the usual solid-state and hydrothermal methods, contains structural defects, namely paramagnetic centers. In accordance with the literature data, MChT of titanium oxide compositions can be accompanied by the reduction of titanium and the formation of a pair  $Ti^{3+}$  - oxygen vacancy  $V_o$  on the surface (Phan et al., 2013; Kolodiazhnyi and Petric, 2003). The EPR spectra of the BT sample obtained by mechanochemical method contain an asymmetric signal with a g factor of 1.970 (Fig. 3), which is attributed to  $Ti^{3+}$  -  $V_o$ , i.e. centers  $Ti^{3+}$  -  $F^+$  (where  $F^+$  is an electron localized at an oxygen vacancy) (Phan et al., 2013). It should be noted that these paramagnetic centres are not recorded for samples treated in water. It is possible that they can be deactivated owing to interaction with molecules of water.

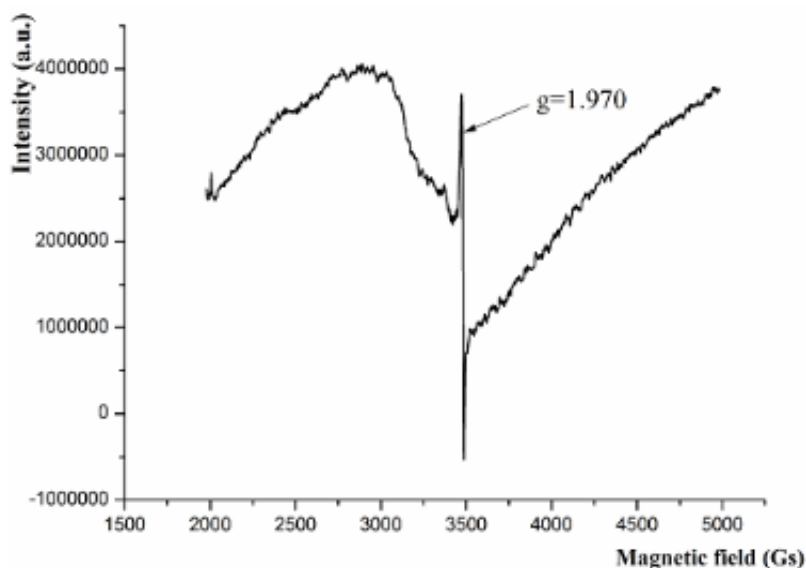


Fig. 3. EPR spectrum for sample MChS-600-air

FTIR spectra recorded in the range 1250-4000 cm<sup>-1</sup> show presence impurities at surface (Fig. 4). Thus, the bands at 1445 and 1350 cm<sup>-1</sup> are related to the vibration of CO<sub>3</sub><sup>2-</sup> groups (Balaz and Plesingerova, 2000) which are always contained in BT synthesized in air and aqueous solutions. The characteristic absorption in the range 3200-3700 cm<sup>-1</sup> is assigned to the stretching vibration of surface OH-groups (Lee et al., 2013; Kaya et al., 2019; Wang et al., 2004). The origin of hydroxyl groups for hydrothermal (after HTT and MWT) and mechanochemical samples is different: they are formed during synthesis in an aqueous medium, in the first case, and they appear during the interaction of

defects, arising during the milling, with air moisture, in the second case. As can be seen, concentration of surface OH-groups is maximal for milled sample.

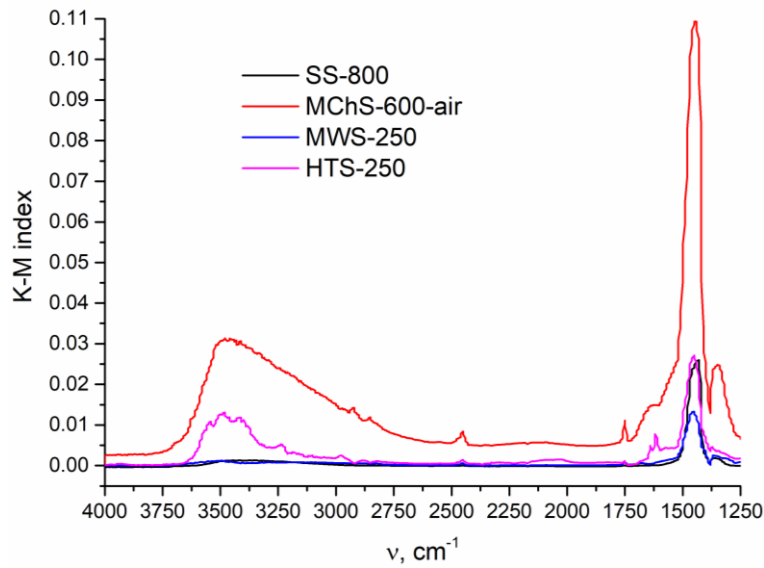


Fig. 4. FTIR spectra for some samples

It should be noted that intensity along the ordinate axis is normalized per unit surface of the samples. Due to this, it can be seen that the content of OH groups is maximum for the sample MChS-600-air. The latter is associated with presence of defects on the surface of this milled sample as above mentioned in the discussion of EPR spectroscopic results.

### 3.2. Electronic structure

Reflectance UV-Vis spectra for all studied samples are presented in Fig. 5a. Absorption edge  $\lambda$  for BT prepared by standard solid-state method (SS-800) is located at 380 nm (Table 2). Red shift of absorption edge (towards visible region) takes place due to treatment of this sample in water (samples SS-MWT-250, SS-MChT-600 H<sub>2</sub>O). The same is observed for samples prepared by direct synthesis from mixture of titanium and barium oxides. Maximum red shift (to 434 nm) was recorded for sample MChS-600-air. Example of Tauc plot for determination of band gap is shown in inset to Fig. 5b. As a result, the narrowing the band gap  $E_g$  occurs for all modified samples compared with solid-state sample. Besides, milled samples (SS-MChT-H<sub>2</sub>O and MChS-600-air) show significant increase of absorption in visible region. Thus, absorption at 568 nm (maximum in the emission spectrum of lamp used for visible irradiation)  $A_{568}$  is 30% for sample MChS-600-air while this value is only 7% for standard solid-state sample SS-800. To explain this experimental fact, it is necessary to consider that

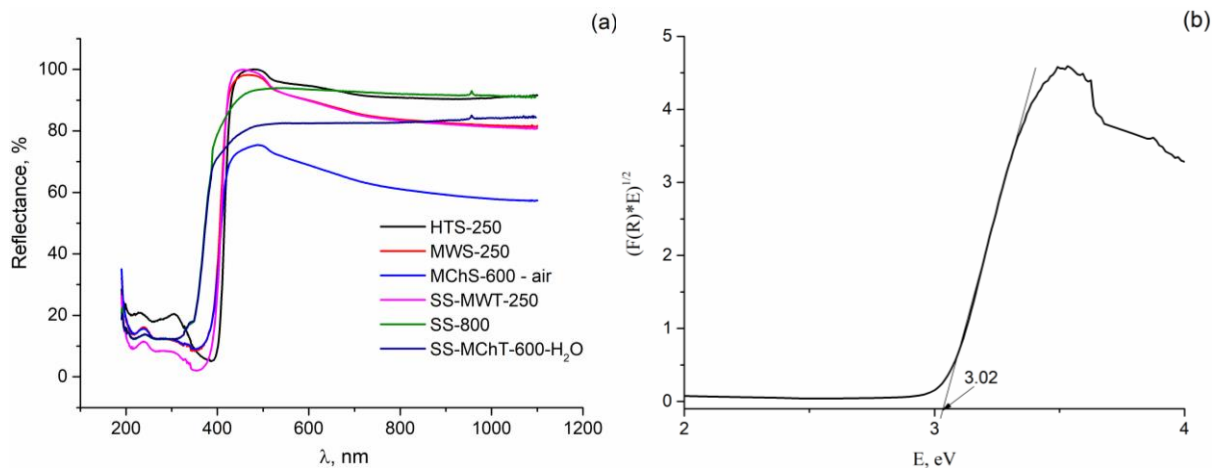


Fig. 5. UV-Vis spectra for studied samples: reflectance (a), Tauc plot for sample SS-MWT-250 (b)

the absorption of radiation by semiconductors depends, among other things, on the presence of defects and internal stresses in the structure (Indris et al., 2005; Gesenhues, 2007), which arise both during mechanochemical treatment.

Table 2. Electronic and photocatalytic properties of studied samples

No.	Designation	$\lambda$ , nm	$E_g$ , eV	$A_{568}$ , %	$a$ , %	$K_d 10^5, s^{-1}$	C, %
1	SS-800	380	3.26	7	22	-	-
2	MChS-600-air	434	2.86	30	41	5.0	85/46
3	MWS-250	417	2.97	10	28	2.1	61/22
4	SS-MChT-600-H2O	391	3.17	18	33	1.1	50/12
5	HTS-250	426	2.91	6	36	3.3	78/39
6	SS-MWT-250	410	3.02	10	31	2.6	69/30

### 3.3. SEM study

Fig. 6. shows the SEM micrographs of BT samples prepared by different methods. Differences in morphology and particle size are noticeable. The mechanochemical sample has the smallest particles that are least aggregated among themselves (image *a*), which is typical for this method of preparation (Ashiri, 2016; Phan et al., 2013). As in works (Lee et al., 2013; Cui et al. 2013), BT particles are agglomerates of spherical shape. The analysis of images *a*, *b*, on the one hand, and *c*, *d*, on the other hand, shows an increase in particle size for hydrothermal samples compared with sample milled in air (Lee et al., 2013; Bantawal and Bhat, 2018; Jiao et al., 2018). This is due to the processes of dissolution-precipitation occurring under hydrothermal conditions, which lead to the enlargement of particles and their coalescence with each other.

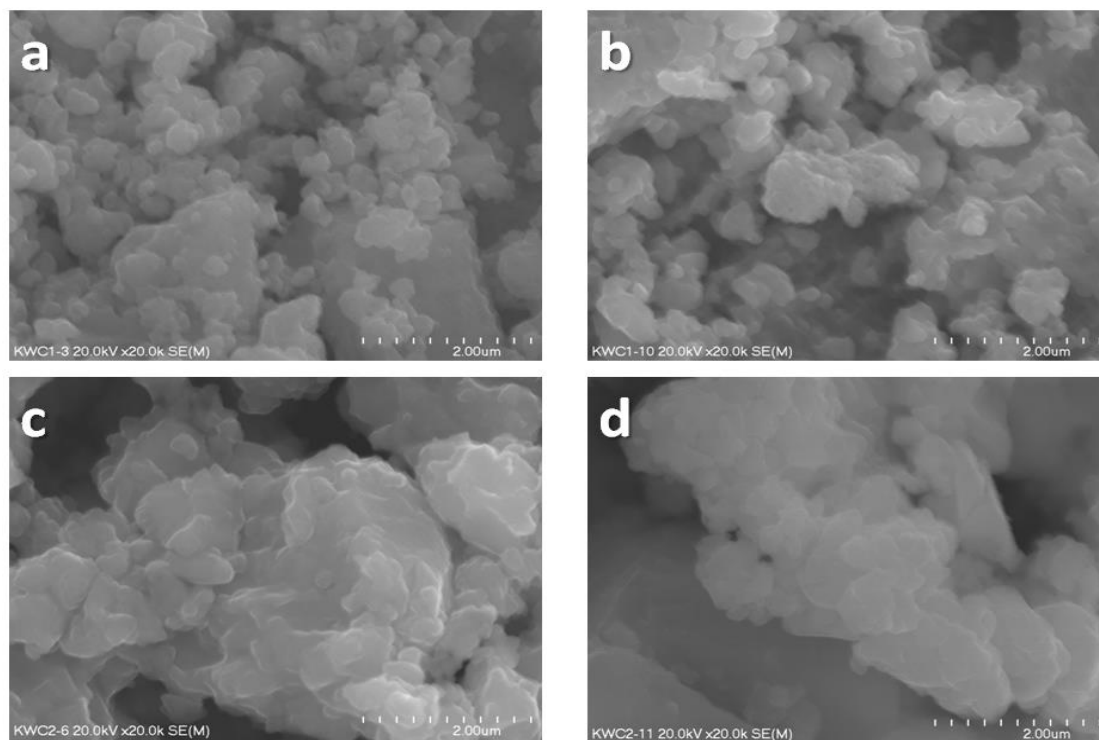


Fig. 6. SEM images for samples MChS-600-air (a), SS-800 (b), MWS-250 (c), HTS-250 (d)

### 3.4. Electrokinetic properties in aqueous dispersions

The dependence of the  $\zeta$ -potential of dispersions of barium titanate powders, prepared by different methods, in water on pH is presented in Fig. 7. As mentioned above, this characteristic is important, since BT is promising in the processes of adsorption of cations as well substrates in photocatalytic processes in an aqueous medium. It can be seen that the value of the  $\zeta$ -potential has a positive value and is quite high (20-60 mV) at pH in the acidic region for all studied dispersions. This is due to the force of electrostatic repulsion arising at the surface of the solid/ solution interface. Since BaTiO<sub>3</sub> powder manifests itself as both a simple insoluble oxide and a partially soluble inorganic salt, the  $\zeta$ -potential is determined by both H<sup>+</sup> and OH<sup>-</sup> ions and Ba<sup>2+</sup>, where the latter's contribution to the surface charge is more significant. With an increase in pH in the range of 2.0-6.5, the  $\zeta$ -potential of all samples decreases to -20(-22) mV, which is consistent with the data of studies (Lewis, 2000; Vamvakaki et al., 2001; Shen et al., 2004). In the pH range 2-6, the value of the  $\zeta$ -potential decreases as follows: SS-800 < MChS-600-air < HTS-250 < MWS-250. The isoelectric point  $\text{pH}_{\text{iep}}$  is shifted to a more alkaline region in the same sequence and is: 3.59; 3.62; 4.16; 4.60, respectively. The experimental  $\text{pH}_{\text{iep}}$  values given in the literature are within 2-10 and are determined by the Ba/Ti ratio, the content of barium carbonate and other impurities in BT (Vamvakaki et al., 2001; Shen et al., 2004; Blanco-Lopez et al., 2000). At the same time, the theoretical position of the isoelectric point, determined by extrapolation to zero BaCO<sub>3</sub> content in BT, corresponds to  $\text{pH} \sim 6.5$  (Blanco-Lopez et al., 2000). It can be seen from the Fig. 7. that the isoelectric point is shifted towards higher pH values (curves 3, 4) for the samples prepared in an aqueous medium (by means of HTT and MWT) compared with solid-state samples (curves 1, 2). The latter is obviously associated with the enrichment of the surface of BT powders with barium cations and, accordingly, with Bronsted basic Ba-OH centers, which occurs due to the leaching of barium in aqueous medium (Shen et al., 2004; Hsu et al., 2005). At  $\text{pH} > 6.5$ , the value of the  $\zeta$ -potential is practically constant and the same for BT of different origin.

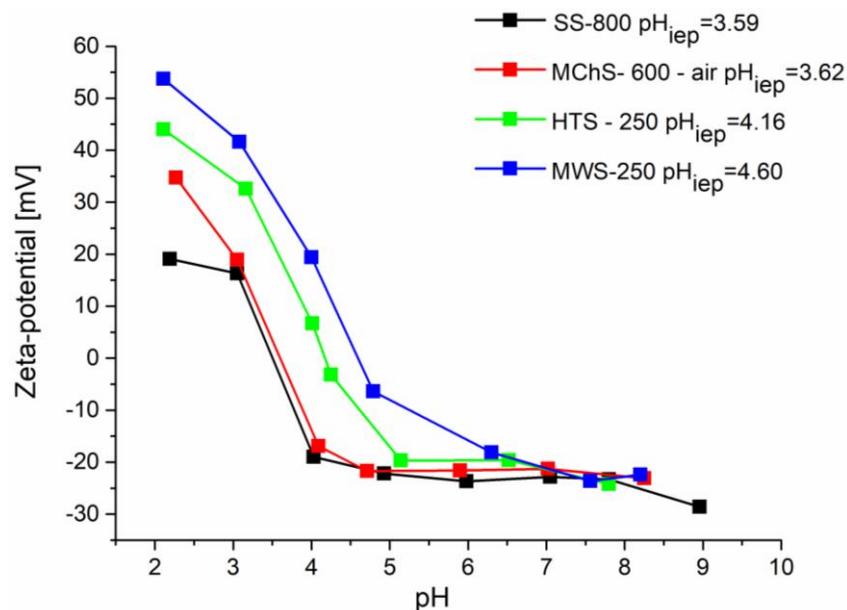


Fig. 7. The dependence of  $\zeta$ -potential from pH for some samples

Fig. 8. presents the exemplary surface charge density as a function of pH in water. It is evident that the content of positively charged groups on the BT surface significantly decreases for all samples with the increasing pH values to 10. Above pH 10, the surface of solid-state samples becomes negatively charged. The point of zero charge  $\text{pH}_{\text{pzc}}$  is 9.94 and 10.22 for SS-800 and MChS-600-air, respectively. At the same time, surface charge density for samples prepared in aqueous medium has a positive value throughout the studied pH range but has a minimum at pH about 10.2-10.3. This indicates the presence of Ba-OH groups on the surface of BT crystallites. The large difference between  $\text{pH}_{\text{iep}}$  and  $\text{pH}_{\text{pzc}}$  cannot be explained from the known data (Kosmulski, 2004) and further studies are needed.

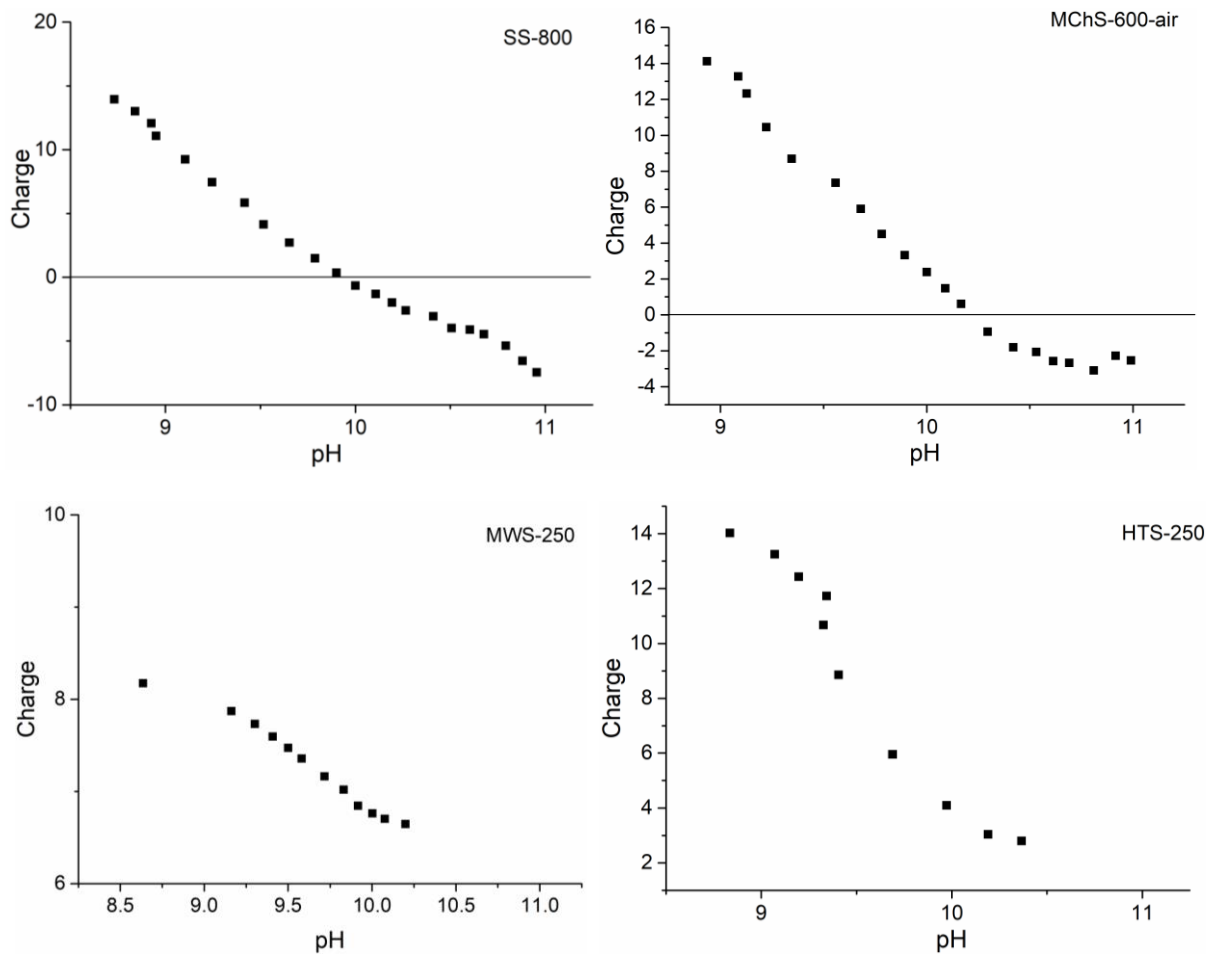


Fig. 8. The dependence of surface charge density from pH for some samples (sample  $\text{BaTiO}_3$  SS-800 and HTT=HTS-250)

### 3.5. Electrokinetic properties in the presence of Cd (II) ions

Fig. 9. presents zeta potential dependence on pH value measured for obtained samples with different Cd (II) concentrations. In general, it can be observed that the more pH increases, the more negative zeta potential becomes. What is more,  $\zeta$ -potential values are influenced by cadmium ions concentrations, namely when Cd(II) amount decreases, the zeta potential becomes lower. It should be noted that for samples with  $10^{-3}$  M Cd(II) it is problematic to estimate general tendency. The potential does not seem to be pH dependent. Some ups and downs are visible on mentioned graphs. The pH range is also limited due to precipitation phenomenon at about pH=8.7, which could be cadmium hydroxide (Luo et al., 1992). Furthermore, the deviating higher values of  $\zeta$ -potential can be seen in other samples with smaller Cd(II) concentrations at pH=6 and 8. Considering all graphs, zeta potential values are in range from approx. -50 mV to -5 mV. It is a significant difference in reference to measurements without cadmium ions. Due to the fact that suspensions are stable, when  $\zeta$ -potential is equal at least +/- 30 mV, only following samples exhibit proper stability: SS-800 with  $10^{-6}$  M Cd(II) above pH=4 and  $10^{-4}$  M Cd(II) above 7, MChS-600-air with  $10^{-6}$  and  $10^{-5}$  M Cd(II) above pH=6, MWS-250 with  $10^{-6}$  and  $10^{-5}$  M Cd(II) above pH=4, HTS-250  $10^{-6}$  and  $10^{-5}$  M Cd(II) in the range of pH=4-5 and above pH=6, SS-MWT-250 with  $10^{-6}$  and  $10^{-5}$  M Cd(II) above pH=6. Moreover,  $\text{pH}_{\text{Iep}}$  is shifted towards acidic area and its value is lower than 3 for each material.

### 3.6. Photocatalytic activity

Photocatalytic properties of semiconductor oxides depend on many factors (Thompson and Yates, 2006; Diebold, 2003). First of all, value of band gap is a prerequisite for the manifestation of activity under visible light. If band gap is lower than 3.26 eV, formation of reactive oxygen species at surface

of semiconductor and initiation of oxidation substrate transformation is possible. As can be seen from Table 2, all samples, excluding SS-800, meet this requirement. It is also natural that the first stage of catalysis is the adsorption of reagents on the catalyst surface. Important parameter of a photocatalyst

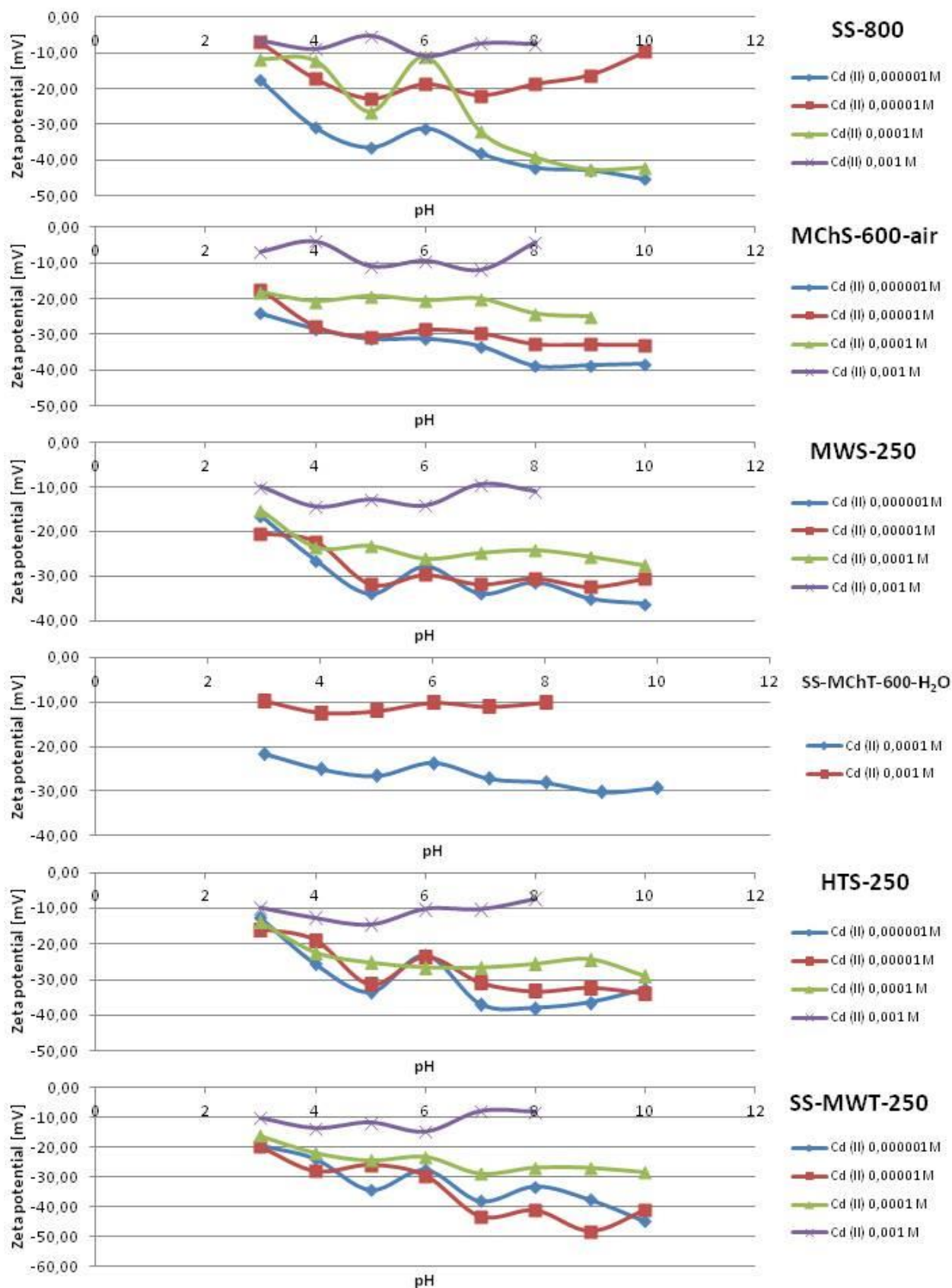


Fig. 9. Zeta potential measured for samples influenced by various Cd(II) concentrations

also is its surface charge in an aqueous medium since it determines character of substrate adsorption. Since the molecule of RhB contains both the basic and acidic groups, it can be adsorbed on the surface in different ways depending on surface charge and pH of RhB solution (Chen et al., 2003). The pH value of RhB initial solution is 6.2 and pH<sub>iep</sub> for tested catalysts is within 3.59-4.60 (Fig. 7). Therefore, the surface of BT samples is negatively charged under degradation conditions. Accordingly, due to the electrostatic interaction, adsorption of RhB molecules on the surface of BT photocatalysts is through positively charged diethylamino groups. As in the case of TiO<sub>2</sub>/SiO<sub>2</sub> photocatalyst (Chen et al., 2003), this provides significant dark adsorption of RhB on the BT surface (Table 2). Also, the adsorption modes of RhB on the surface of catalysts greatly influence the photocatalytic degradation mechanism of the RhB (Wilhelm and Stephan, 2007; Chen et al., 2003). As can be seen from Table 2, the value of RhB adsorption on dark stage *a* (%) differ quite strongly since tested samples have different specific surface area (Table 1) and degree of surface hydroxylation (Fig. 4).

The RhB degradation was estimated from the decrease in the intensity (optical density) of the band at 553 nm in absorption spectra of RhB solutions. It was found that, in all cases, the photodegradation (bleaching) rate of the dye is satisfactorily described by a first-order kinetic equation ( $R^2 = 0.93-0.98$ ) as in works (Demydov and Labaunde, 2004; Khalameida et al., 2010; Lee et al., 2013; Kaya et al., 2019). Examples of kinetic curves of RhB photocatalytic degradation as well as its photolysis (blank experiment without catalyst) are shown in Fig. 10.

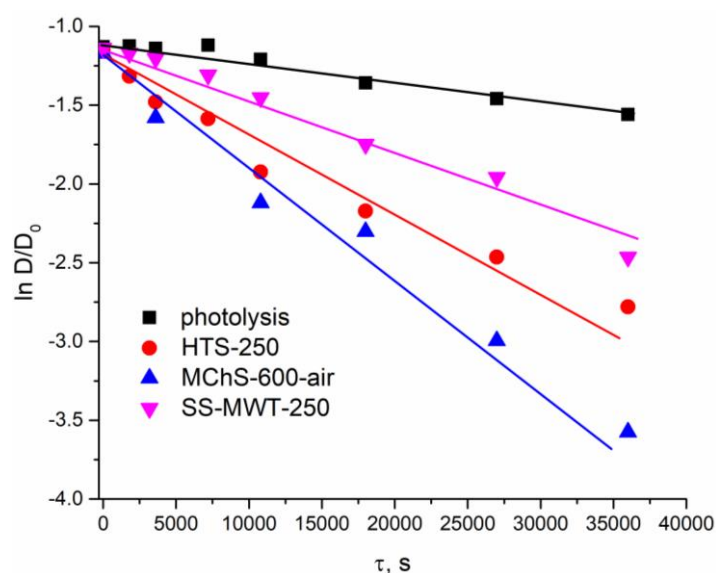


Fig. 10. Kinetic curves of RhB photolysis and photocatalytic degradation using some studied samples

The photodegradation rate constant  $K_d$ , calculated from the dependence optical density – time of illumination. Despite the higher surface area, the solid state sample SS-800 showed the lowest dye adsorption and was found to be inactive under visible irradiation. The first is associated with dehydroxylation of the surface at high temperature calcinations (800°C), and the second with a high value of the band gap. All other samples exhibit noticeable photocatalytic activity although less than under UV illumination (Khalameida et al., 2010). The most active is the sample MChS-600-air, which is characterized by a set of favorable characteristics: a sufficiently high specific surface area, the maximum content of surface OH-groups, absorption of visible light, and a low band gap. Its activity is comparable with that obtained for RhB photocatalytic degradation under solar irradiation using barium titanate prepared by solid state way (Cui et al., 2013):  $5 \cdot 10^{-5} \text{ s}^{-1}$  in first case against  $2 \cdot 10^{-5} \text{ s}^{-1}$  for cubic barium titanate and  $6 \cdot 10^{-5} \text{ s}^{-1}$  for tetragonal barium titanate in second case. The course of a photocatalytic reaction occurs according to usual free radical mechanism with formation of reactive oxygen species which was earlier described for barium titanate (Lee et al., 2013; Ni et al., 2015; Pirgholi-Givi et al., 2021; Xiong et al., 2015). Under irradiation, these processes are initiated by excitation of an electron-hole pair on the surface or photosensitization of dye molecules. The latter is characteristic for rhodamine B (Wilhelm and Stephan, 2007; Cui et al., 2013).

The photocatalytic activity as degree of degradation C (in %) was estimated: /i/ degree of bleaching the RhB solution (in %) using reduction in intensity of band at 553 nm; /ii/ the degree of RhB mineralization was also calculated based on changes in total organic carbon (TOC) (Rauf and Ashraf, 2009). The second indicator is more important from a practical point of view since it characterizes transformation of organic pollutants into less harmful inorganic substances. Both parameters are presented through a fraction (bleaching/mineralization) in the last column of the Table 2. One can see that degree of bleaching is within 50-85% while degree of mineralization is much less. The latter is due to the fact that deethylation of RhB to Rh110 obviously occurs as described earlier (Wilhelm and Stephan, 2007; Chen et al., 2003). In addition, it is known that the degree of demineralization of dyes in solutions is always less than the degree of their discoloration (Rauf and Ashraf, 2009).

#### 4. Conclusions

The samples of barium titanate were prepared by four different procedures. All prepared samples have structure of barium titanate cubic modification. Specific surface area of studied samples is within 6-23 m<sup>2</sup>/g as in other works devoted barium titanate. EPR spectroscopy indicates that mechanochemical BT, in contrast to samples prepared by the usual solid-state and hydrothermal methods, contains structural defects, namely paramagnetic centers. FTIR spectra recorded in the range 1250-4000 cm<sup>-1</sup> show presence impurities at surface. The origin of hydroxyl groups for hydrothermal (after HTT and MWT) and mechanochemical samples is different: they are formed during synthesis in an aqueous medium, in the first case, and they appear during the interaction of defects, arising during the milling, with air moisture, in the second case. The SEM micrographs of BT samples prepared by different methods, as in works particles are agglomerates of spherical shape. The isoelectric point p*H*<sub>iep</sub> is shifted to a more alkaline region in the same sequence and is: 3.59; 3.62; 4.16; 4.60, respectively. The point of zero charge p*H*<sub>pzc</sub> is 9.94 and 10.22 for SS-800 and MChS-600-air, respectively. ζ-potential values are influenced by cadmium ions concentrations, namely when Cd(II) amount decreases, the zeta potential becomes lower. zeta potential values are in range from approx. -50 mV to -5 mV. It is a significant difference in reference to measurements without cadmium ions. Photocatalytic activity under visible irradiation was shown by all samples, with the exception of the sample prepared *via* solid state reaction at high temperature. First of all, this is due to the narrowing of the band gap as well as maximum in surface OH-groups content. The obtained result firstly show relationship between the conditions of barium titanate synthesis, its physicochemical and electrokinetic parameters, as well as photocatalytic activity under visible light. As a result, they convincingly demonstrate the possibility of using synthetic (and apparently spent) barium titanate in water purification processes.

#### References

- ASHIRI, R., 2016. *On the solid-state formation of BaTiO<sub>3</sub> nanocrystals from mechanically activated BaCO<sub>3</sub> and TiO<sub>2</sub> powders: innovative mechanochemical processing, the mechanism involved, and phase and nanostructure evolutions.* RSC Advances, 6, 17138–17150.
- AL-HOBAIB, A.S., AL-SUHYBANI, A.A., 2014. *Removal of uranyl ions from aqueous solutions using barium titanate.* J Radioanal Nucl Chem 299, 559–567.
- BAGHERI, H., FAKHRI, H., GHAHREMANI, R., KARIMI, M., MADRAKIAN, T., AFKHAMI, A. 2020. *Nanomaterial-based adsorbents for wastewater treatment.* Smart Nanocontainers, 467–485.
- BALAZ, P., PLESINGEROVA, B., 2000. *Thermal properties of mechanochemically pretreated precursors of BaTiO<sub>3</sub> synthesis.* J Therm Anal Calorim. 59, 1017–21.
- BANTAWAL, H., BHAT, D.K., 2018. *Hierarchical Porous BaTiO<sub>3</sub> Nano-Hexagons as A Visible Light Photocatalyst.* International Journal of Engineering & Technology 7, 105-109.
- BLANCO-LOPEZ, M.C., RAND, B., RILEY, F.L., 2000. *The isoelectric point of BaTiO<sub>3</sub>.* J. Eur. Ceram. Soc. 20. 107-118.
- CHEN, F., ZHAO, J., HIDAKA, H., 2003. *Highly selective deethylation of rhodamine B: Adsorption and photooxidation pathways of the dye on the TiO<sub>2</sub>/SiO<sub>2</sub> composite photocatalyst.* International Journal of Photoenergy 5(4), 209–217.

- CHEN, Y.-H., CHEN, Y.-D., 2011. *Kinetic study of Cu(II) adsorption on nanosized BaTiO<sub>3</sub> and SrTiO<sub>3</sub> photocatalysts*. *Journal of Hazardous Materials*, 185, 168–173.
- CHUN, H., YIZHONG, W., HONGXIAO, T. 2001. *Influence of adsorption on the photodegradation of various dyes using surface bond-conjugated TiO<sub>2</sub>/SiO<sub>2</sub> photocatalyst*. *Applied Catalysis B: Environmental* 35(2), 95–105.
- CUI, Y., BRISCOE, J., DUNN, S., 2013. *Effect of Ferroelectricity on Solar-Light-Driven Photocatalytic Activity of BaTiO<sub>3</sub> – Influence on the Carrier Separation and Stern Layer Formation*. *Chemistry of Materials* 25(21), 4215–4223.
- DEMYDOV, D., LABAUNDE, K.J., 2004. *Characterization of mixed metal oxides SrTiO<sub>3</sub> and BaTiO<sub>3</sub> synthesized by a modified aerogel procedure*. *J. Non-Cryst. Solids*. 350, 165-172.
- DIEBOLD, U., 2003. *The surface science of titanium dioxide*. *Surf. Sci. Rep.* 48, 53–229.
- GESENHUES, U., 2007. *The effects of plastic deformation on band gap, electronic defect states and lattice vibrations of rutile*. *J. Phys. Chem. Solids* 68, 224-235.
- GORELOV, B.M., KOTENOK, E.V., MAKHNO, S.N., SYDORCHUK, V.V., KHALAMEIDA, S.V., ZAZHIGALOV, V.A., 2011. *Structure and optical and dielectric properties of barium titanate nanoparticles obtained by the mechanochemical method*. *Techn. Phys.* 56, 83–91.
- GÓRSKA, P., ZALESKA, A., KOWALSKA, E., KLIMCZUK, T., SOBCZAK, J. W., SKWAREK, E., HUPKA, J., 2008. *TiO<sub>2</sub> photoactivity in vis and UV light: The influence of calcination temperature and surface properties*. *Applied Catalysis B: Environmental* 84(3-4), 440–447.
- GUEVAR, C., HERTZ, A., BRACKX, E., BARRE, Y., GRANDJEAN, A., 2017. *Mechanisms of strontium removal by a Ba-titanate material for the wastewater treatment*. *Journal of Environmental Chemical Engineering* 5, 4948-4957.
- GUIN, R., DAS, S. K., SAHA, S. K., 2002. *Adsorption studies of zinc ions on barium titanate from aqueous solution*. *Radiochimica Acta* 90(1), 53-56.
- HSU, R.C., YING, K.L., CHEN, L.P., 2005. *Dispersion properties of BaTiO<sub>3</sub> colloids with amphoteric polyelectrolytes*. *J. Amer. Ceram. Soc.* 88, 524-529.
- INDRIS, S., AMADE, R., HEITJANS, P., 2005. *Preparation by high- energy milling, characterization, and catalytic properties of nanocrystalline TiO<sub>2</sub>*. *J. Phys. Chem. B.* 109, 23274-23278.
- JANUSZ, W., KHALAMEIDA, S., SYDORCHUK, V., SKWAREK, E., ZAZHIGALOV, V., SKUBISZEWSKA-ZIĘBA, J., LEBODA, R., 2010. *Some properties of milled vanadium phosphates*. *Adsorption*. 16, 333–341.
- JIAO, H., ZHAO, K., MA, L., TANG, Y., 2016. *A simple one-step hydrothermal synthesis and photocatalysis of bowl-like BaTiO<sub>3</sub> nanoparticles*. *Inorganic and Nano-Metal Chemistry* 47(5), 647–654.
- KAPPADAN, S., GEBREAB, T. W., THOMAS, S., KALARIKKAL, N., 2016. *Tetragonal BaTiO<sub>3</sub> nanoparticles: An efficient photocatalyst for the degradation of organic pollutants*. *Materials Science in Semiconductor Processing* 51, 42–47.
- KARTHIK, K. V., REDDY, C. V., REDDY, K. R., RAVISHANKAR, R., SANJEEV, G., KULKARNI, R. V., RAGHU, A. V., 2019. *Barium titanate nanostructures for photocatalytic hydrogen generation and photodegradation of chemical pollutants*. *Journal of Materials Science: Materials in Electronics* 30(23), 20646-20653.
- KAYA, I.C., KALEM, V., AKYILDIZ, H., 2019. *Hydrothermal synthesis of pseudocubic BaTiO<sub>3</sub> nanoparticles using TiO<sub>2</sub> nanofibers: Study on photocatalytic and dielectric properties*, *Int J Appl Ceram Technol.* 16, 1557–1569.
- KHALAMEIDA, S. V., SYDORCHUK, V. V., ZAZHIGALOV, V. A., MIRONYUK, T. I., 2010. *Specific features of the photocatalytic destruction of Safranin T on mechanochemically produced barium titanate*. *Russian Journal of Applied Chemistry* 83(10), 1799–1803.
- KHALAMEIDA, S., SYDORCHUK, V., SKUBISZEWSKA-ZIĘBA, J., LEBODA, R., ZAZHIGALOV, V., 2010. *Synthesis, thermoanalytical, and spectroscopical studies of dispersed barium titanate*. *Journal of Thermal Analysis and Calorimetry* 101(2), 779–784.
- KHALAMEIDA, S., SYDORCHUK, V., ZAZHIGALOV, V., WIECZOREK-CIUROWA, K., SKUBISZEWSKA-ZIĘBA, J., CHARMAS, B., 2017. *The Interaction between Barium and Titanium Oxides under Mechanochemical, Hydrothermal and Microwave Treatments and Properties of Prepared Products*. *Advanced Science, Engineering and Medicine* 9, 235-246.
- KIKUTA, K., SHIMIZU, Y., MORIYA, M., YAMAGUCHI, T., HIRANO, S., SAITO, Y., SAKABE, Y., 2006. *Low Temperature Recycling Process for Barium Titanate Based Waste*. *Journal of the Ceramic Society of Japan* 114(1329), 392–394.
- KOLODIAZHNYI, T., PETRIC, A., 2003. *Analysis of point defects in polycrystalline BaTiO<sub>3</sub> by electron paramagnetic resonance*. *Journal of Physics and Chemistry of Solids* 64(6), 953–960.

- KOSMULSKI, M., 2004. *pH-dependent surface charging and points of zero charge II. Update*. Journal of Colloid and Interface Science 275(1), 214–224.
- LANDRI, S.Jr., SEGUNDO, I.R., FREITAS, E., VASILESKIY, M., CARNEIRO, J., TAVARES, C.J., 2022. *Use and misuse of the Kubelka-Munk function to obtain the band gap energy from diffuse reflectance measurements*. Solid State Communications 3341, 114573.
- LEE, W. W., CHUNG, W.H., HUANG, W.S., LIN, W.C., LIN, W.Y., JIANG, Y.R., CHEN, C.C., 2013. *Photocatalytic activity and mechanism of nano-cubic barium titanate prepared by a hydrothermal method*. Journal of the Taiwan Institute of Chemical Engineers 44(4), 660–669.
- LEWIS, J.A., 2000. *Colloidal processing of ceramics*. J. Amer. Ceram. Soc. 83(10), 2341-2359.
- LUO, B., PATTERSON, J.W., ANDERSON, P.R., 1992. *Kinetics of cadmium hydroxide precipitation*, Water Research 26(6), 745-751.
- MALGHE, Y.S., GURJAR, A.V., DHARWADKAR, S.R., 2004. *Synthesis of BaTiO<sub>3</sub> powder from barium titanate oxalate (BTO) precursor employing microwave heating technique*. Bull. Mater. Sci. 27, 217.
- MISHRA, S.P., SINGH, V.K., TIWARI, D., 1996. *Radiotracer technique in adsorption study. Pt. 15. Removal behaviour of barium titanate for mercury ions*. Radiochimica Acta 73(1), 49-53.
- NI, Y., ZHENG, H., XIANG, N., YUAN, K., HONG, J., 2015. *Simple hydrothermal synthesis and photocatalytic performance of coral-like BaTiO<sub>3</sub> nanostructures*. RSC Advances 5(10), 7245–7252.
- PHAN, T.L., ZHANG, P., YANG, D. S., THANH, T. D., TUAN, D. A., YU, S.C., 2013. *Origin of ferromagnetism in BaTiO<sub>3</sub> nanoparticles prepared by mechanical milling*. Journal of Applied Physics 113(17), 17E305.
- PIRGHOLI-GIVI, G., AZIZIAN-KALANDARAGH, Y., FARAZIN, J., 2021. *Comparison of the photocatalytic activity of perovskite structures: Bismuth, barium, and zinc titanate nanostructures for photodegradation of methylene blue from water*. Journal of Photochemistry and Photobiology A: Chemistry 408, 113104.
- RAE, A., CHU, M., GANINE, V., 2007. *Barium titanate: past, present and future*. Ceram Trans. 100, 1–12.
- RAUF, M.A., ASHRAF, S.S., 2009. *Fundamental principles and application of heterogeneous photocatalytic degradation of dyes in solution*, Chem. Eng. J. 151. 10–18.
- SAITO, T., SHIRAIWA, N., MORIOKA, Y., AKAGI, K., NAKAYAMA, K. S., ADSCHIRI, T., ASAO, N., 2019. *Granular Barium Titanate Nanowire-Based Adsorbents for the Removal of Strontium Ions from Contaminated Water*. ACS Applied Nano Materials 2(11), 6793-6797.
- SARAVAIA, H., GUPTA, H., KULSHRESHTHA, V., 2016. *Synthesis of Nano-Barium Titanate and Application for Strontium Adsorption from Aqueous Solution*. Advanced Materials Research 1141, 190–195.
- SHEN, Z.G., CHEN, J.F., ZOU, H.K., YUN, J., 2004. *Dispersion of nanosized aqueous suspensions of barium titanate with ammonium polyacrylate*. J. Colloid Interface Sci. 275, 158-164.
- SYDORCHUK, V. V., ZAZHIGALOV, V. A., KHALAMEIDA, S. V., WIECZOREK-CIUROWA, K., SKUBISZEWSKA-ZIĘBA, J., LEBODA, R., 2009. *Investigation of physicochemical transformation at mechanochemical, hydrothermal and microwave treatment of barium titanate oxalate*. Journal of Alloys and Compounds 482(1-2), 229–234.
- THOMPSON, Tracy L., YATES, JOHN T., 2006. *Surface science studies of the photoactivation of TiO<sub>2</sub> new photochemical processes*. Chemical reviews 106, 4428-4453.
- TRIPATHY, S.S., RAICHUR, A.M., 2011. *Dissolution properties of BaTiO<sub>3</sub> nanoparticles in aqueous suspensions*, Journal of Experimental Nanoscience 6(2), 127-137.
- VAMVAKAKI, M., BILLINGHAM, N. C., ARMES, S. P., WATTS, J. F., GREAVES, S. J., 2001. *Controlled structure copolymers for the dispersion of high-performance ceramics in aqueous media*. Journal of Materials Chemistry 11(10), 2437-2444.
- WANG, J., YIN, S., KOMATSU, M, M., ZHANG, Q., SAITO, F., SATO, T., 2004. *Photo-oxidation properties of nitrogen doped SrTiO<sub>3</sub> made by mechanical activation*. Appl. Catal. B 52(1), 11-21.
- WELHAM, N. J., 1998. *Mechanically induced reaction between alkaline earth metal oxides and TiO<sub>2</sub>*. Journal of Materials Research 13(06), 1607–1613.
- WILHELM, P., STEPHAN, D., 2007. *Photodegradation of rhodamine B in aqueous solution via SiO<sub>2</sub>@TiO<sub>2</sub> nano-spheres*. Journal of Photochemistry and Photobiology A: Chemistry 185(1), 19–25.
- XIONG, X., TIAN, R., LIN, X., CHU, D., LI, S., 2015. *Formation and Photocatalytic Activity of BaTiO<sub>3</sub> Nanocubes via Hydrothermal Process*. Journal of Nanomaterials, 2015, 1–6.
- ZAZHIGALOV, V.A., SIDORCHUK, V.V., KHALAMEIDA, S.V., KUZNETSOVA, L.S., 2008. *Mechanochemical synthesis of BaTiO<sub>3</sub> from barium titanate oxalate*. Inorg Mater 44, 641-645.